Heliyon 7 (2021) e06053

Contents lists available at ScienceDirect

Heliyon

journal homepage: www.cell.com/heliyon

Review article

Forced flow cryogenic cooling in fusion devices: A review

Hitensinh Vaghela [a,b,*], Vikas J. Lakhera [b], Biswanath Sarkar [a]

[a] ITER-India, Institute for Plasma Research, Ahmedabad, 380005, India
[b] Institute of Technology, Nirma University, Ahmedabad, 382481, India

ARTICLE INFO

Keywords:
Fusion
Superconducting magnets
Cryogenics
Thermo-hydraulic
CICC
Cryopump

ABSTRACT

The constantly increasing energy consumption along with the depleting fossil fuel resources as well as owing to the fact that the nuclear fission not being an intrinsically safe method of energy generation, it has become necessary to look for other solutions to fulfil the future energy demands. Nuclear fusion, the source of energy for billions of stars, has attracted the attention of scientists and engineers despite a lot of technical challenges in the replication of the fusion process in laboratories. For fusion to take place in a device, one of the major challenges faced is the strong magnetic confinement of the plasma using large superconducting (SC) magnets, which need efficient cryogenic cooling techniques to maintain the required low temperatures for the superconducting state. In order to maintain the compactness, the SC magnets generally employ Cable in Conduit Conductor (CICC) windings, carrying high current densities, which are cooled by the forced flow of helium at ~4 K temperature to maintain the required superconducting temperatures. The construction of CICC aims to maintain the superconductivity state by optimization of various parameters such as thermal stability, the ratio of normal conductor to SC material, mechanical strength, low hydraulic impedance, current density, magnetic field, etc. The cryogenic thermal stability of the CICC is of prime importance for safe, stable and reliable operation of SC magnets. The prediction of thermal and hydraulic behavior of the CICC in large SC magnets is difficult due to the complex geometry involved, the variation in fluid properties, various heat in-flux incidences over the long length of CICC and a complex heat transport phenomenon. Another application which utilizes a forced flow cryogenic cooling in the fusion devices is a cryo-adsorption pump for creating clean and high vacuum with large pumping speed. This paper presents an overview of the forced flow cryogenic cooling schemes in fusion devices along with a systematic review of the thermal and hydraulic studies related to CICC and cryo-adsorption pump, thereby highlighting the challenges and opportunities for further improvement in their design and performance.

1. Introduction

The world energy demand is expected to increase by several folds mainly due to the population growth and an increase in the per capita consumption of energy. The projections of future energy demand based on the present and past energy trends is shown in Figure 1 [1]. The presently available energy resources include the conventional fossil fuel reserves (coal, oil and natural gas), nuclear fission, solar based sources, hydropower, etc. Among the various options available, conventional fossil fuels are limited and their increasing consumption trends have unfavorable ecological effects. Although the nuclear fission fuel is available naturally, it is not abundant, and its conversion into useful energy has several safety concerns including the nuclear waste disposal. The technological advancements are ongoing with the solar energy option which involves simultaneous improvement in conversion efficiency and energy storage technology. Due to its low power density and an intermittent nature, the use of solar energy as base energy is restricted. The use of hydropower invokes growing concerns of ecological imbalance due to the involvement of large man-made reservoirs. Moreover, favorable geographical conditions are required for setting up a hydropower plant. Hence in order to meet the future energy demand through an eco-friendly way, it is imperative to explore an out of the box solution. One such solution is the nuclear fusion option which is also a source of energy for billions of stars including the sun. The role of nuclear fusion technology for meeting the future energy demand has been acknowledged in several countries including India [2, 3].

There are several ways by which the nuclear fusion can be achieved. One such way is by magnetic confinement of atoms in the ionized form (plasma state) and creating suitable conditions (high kinetic energy, sufficient density and time) for their collision to achieve fusion energy. In

* Corresponding author.
E-mail address: jaihiten@gmail.com (H. Vaghela).

https://doi.org/10.1016/j.heliyon.2021.e06053
Received 17 August 2020; Received in revised form 20 November 2020; Accepted 18 January 2021

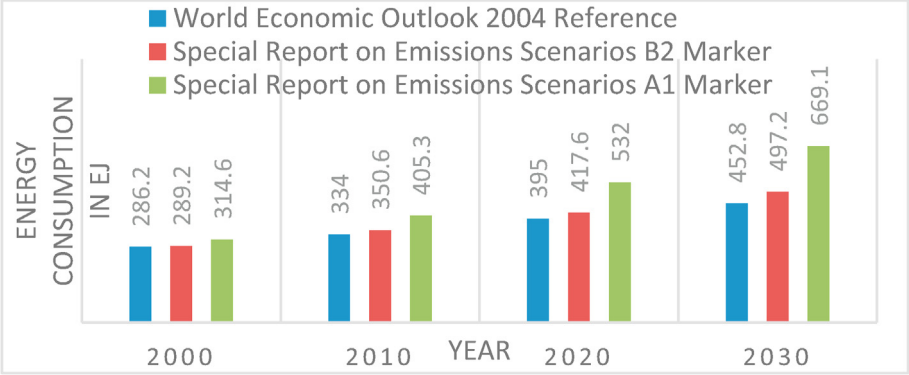

Figure 1. Future energy demand projections.

order to obtain net energy out of the nuclear fusion, strong magnetic confinement necessitates the use of strong magnets which leads to a choice of cryogenically cooled superconducting (SC) magnets. The cryogenic cooling system of SC magnets is an essential part of any magnetically confined fusion device. The SC magnet cooling employs various techniques such as pool/bath cooling and forced flow cooling. The cryogenic cooling is also beneficial and required to achieve high and clean vacuum in the fusion devices by the application of cryopumps. In the present study a state-of-the-art review has been carried out for the forced flow cryogenic cooling, involving thermal and hydraulic aspects, of SC magnets, which use the Cable in Conduit Conductor (CICC), and cryopumps using the Hydraulically Form Dimple Panels (HFDP). The prediction of thermal and hydraulic behavior of CICC in large SC magnets is difficult due to reasons such as the complex geometry involved, the variation in fluid properties, various heat in-flux incident over the long length of CICC and complex heat transport phenomena. Despite a significant advancement in the development of CICC based SC magnets, the prediction of thermal and hydraulic impedance is not yet well established and hence the present challenges are discussed and summarized. This paper presents an overview of the SC magnet based fusion devices, a typical cryogenic cooling scheme of SC magnets in fusion devices along with a systematic review of the thermal and hydraulic studies related to CICC and cryopump, thereby highlighting the challenges and opportunities for further improvement in its design and performance.

2. Nuclear fusion

In nuclear fusion, two nuclei of atoms are brought close enough for a sufficiently long time at a very high-temperature plasma (of the order of hundred million Kelvin) to overcome the repulsive force (Coulomb barrier) and start quantum tunnelling, thereby resulting in a fusing of the nuclei and release of energetic particles, a part of which can be converted into heat [4]. The Deuterium –Tritium (DT) fusion reaction, which releases ~17.6 MeV energy per reaction, is the most favorable reaction due to its high reactivity and lower temperature (~800 Million Kelvin) requirement.

By providing a means to transfer the heat generated from the fusion reaction to the conventional steam power plant, the fusion energy can be converted to electrical energy [5]. Presently, the fusion energy conversion technology is in its initial stages and requires substantial research and development in order to achieve sustainable fusion process thereby paving a path for the development of commercially viable fusion reactors in future. Several countries have initiated research programs related to fusion technology and the development of practically viable fusion devices [6].

The fusion reaction may be achieved in the laboratory either by magnetic confinement or by the inertial confinement approach. The inertial confinement approach achieves fusion by compressing a solid fuel pellet to very high densities by bombarding it with an inertial fusion driver such as lasers, heavy-ion beams, etc. [7]. Figure 2 shows an overview of the various methods to achieve nuclear fusion. The magnetic confinement approach uses external and self-generated magnetic fields in order to hold the plasma at relatively low densities away from material walls for time periods of the order of a few seconds.

3. Magnetic confinement based fusion devices

Among the various methods of achieving fusion, magnetically confined nuclear fusion is a promising option for which various countries have been making efforts paving a way and develop a commercial fusion reactor. Over the last decade, fusion experiments have made enormous strides towards research and development with the goal of achieving energy production from the fusion process.

The most significant achievement in fusion experiments has been in the domain of the magnetic confinement approach. The magnetic confinement can be achieved through two of the most popular methods, namely, the tokamak and the stellarator [8]. The stellarator concept was introduced by Lyman Spitzer in Princeton in 1951, whereas, the first tokamak T-1 was built and tested in Russia during 1958 [9]. The word 'tokamak' is an acronym in Russian, which translates in English as the 'toroidal chamber with magnetic coil'.

In a tokamak, the confinement is achieved by a combination of a toroidal magnetic field, produced by toroidal field coils, and a poloidal magnetic field produced by a toroidal current in the plasma. The plasma current is initiated through a current swing (transformer action) in the central solenoid which acts as a primary winding with the plasma in torus chamber acting as a secondary winding thereby creating the current flow

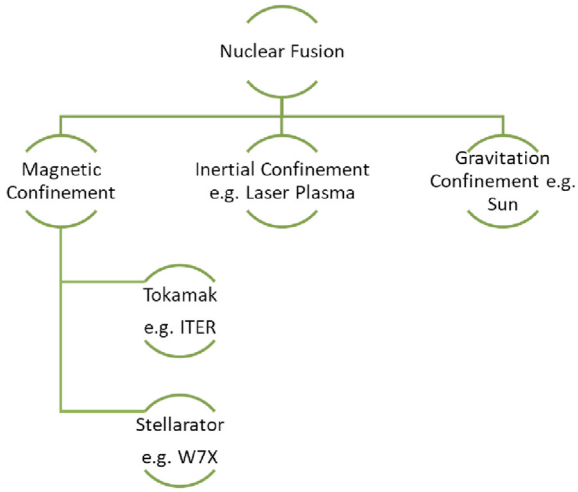

Figure 2. Approaches to achieve nuclear fusion.

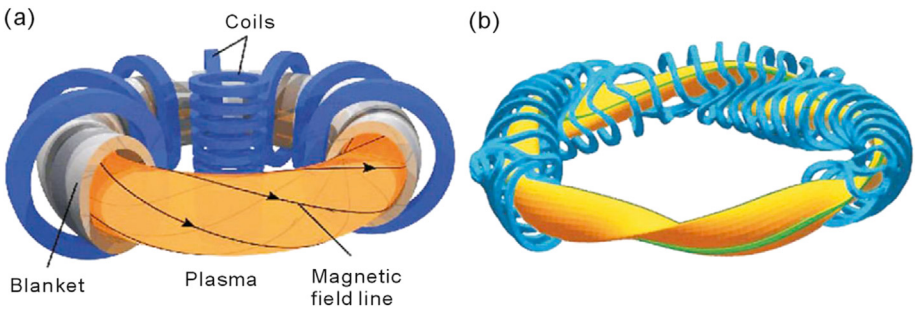

Figure 3. Magnetic confinement of plasma (a) tokamak and (b) stellarator [8].

through the plasma in a toroidal direction. The current flowing through the plasma in the toroidal direction produces a magnetic field in the poloidal direction and as a combined effect of the toroidal field and the poloidal field, a resultant helical field is created. In a stellarator, the twist in the magnetic field is not created by a current swing (transformer action) but by employing specific 3-D shaped helical field coils. The construction and principle of the tokamak and the stellarator are shown schematically in Figure 3[1] [8].

Unlike tokamak, the stellarator operates in a steady-state and produces a helical field by the complex non-axisymmetric shape of magnet coil in order to confine plasma in a toroidal chamber. There are other differences also between the tokamak and stellarator in terms of plasma physics [8], i.e., magneto-hydrodynamic (MHD) instabilities, neoclassical and turbulent transport, plasma confinement, plasmas rotation and edge physics, etc. Both, the tokamak and the stellarator employ SC magnets to create the required high magnetic field and make use of cryogenically cooled CICC in order to achieve magnetic confinement. The major parameters for various SC tokamaks and stellarators worldwide with cryogenic cooling capacities are summarized in Table 1.

4. Cooling requirements for superconducting (SC) magnets

In order to create a high strength magnetic field in magnetic confinement fusion, the use of SC magnets are inevitable [28, 29] and the SC magnets are considered to be one of the most important sub-systems for fusion devices. Due to their very high current densities, high and stable magnetic field, the use of SC magnets is not limited to the magnetic confinement based fusion devices only but also extends to other applications, namely, Magnetic Resonance Imaging (MRI), Nuclear Magnetic Resonance (NMR), particle accelerator and mass spectrometry [30].

The thermal stability of the SC magnets is the essential requirement for successful magnet and cable applications. The stability of the SC magnets is achieved by managing proper cryogenic cooling which overcomes the static and pulsed heat load (AC losses, nuclear heating etc.) as well as other energy inputs to maintain the conductor in a superconducting state.

The stability of the SC magnets is achieved by proper design and manufacturing of SC cable/magnet as well as employing proper cryogenic cooling which overcomes static and pulsed heat load (AC losses, nuclear heating etc.). Other energy inputs such as Joule heating, which is induced when the current in the superconductor exceeds its current carrying capacity and starts a transition towards a normal conductor, need to be considered. This transition initiates Joule heating and current sharing between the SC and stabilizer. The transition can be recovered by the forced flow cooling which overcomes the Joule heating. The transition can be quantified by a power law relation for the electric field in the superconductor and is characterized by an exponent n in the following equation.

$$\frac{E}{E_0} = \left(\frac{I}{I_c}\right)^n \quad \text{Eq. 1}$$

where E_0 is the electric field used as a criterion for the definition of the critical current I_c, n is the exponent defining the sharpness of the transition, E is a longitudinal electric field in the conductor, and I is operating current. In practice, a large number of SC magnets are made of Low-Temperature Superconductor (LTS) with Cable-in-Conduit Conductor (CICC) which are normally cooled with forced flow helium at a temperature level of 4 K [31].

Thus, large superconducting magnet systems, in size and field are inevitable for a fusion device wherein cryogenic cooling plays a vital role to support the efficient operation of SC magnets. The cryogenic system provides necessary cooling power to maintain the magnets in its superconducting state in presence of several disturbances, such as quench, inductive current drive, etc., that arises during the operation of a fusion device.

5. Cryogenic system in fusion devices

The cryogenic system for fusion device can be divided into three main sub-systems, namely, helium refrigerator/liquefier (R/L), distribution system and application system. These three sub-systems typically work in a linked manner, through proper arrangements of components which include warm compressors, heat exchangers (HXs), turboexpanders, cryogenic valves, phase separator, cold circulator, cold compressor as well as interconnecting pipes as shown schematically in Figure 4 for a typical cryogenic system in fusion device.

The helium R/L is conventionally designed to operate in a steady-state operating mode, i.e., the heat load fluctuations from applications must be smoothened. The steady-state operation is required because any conventional liquid helium (LHe) plant becomes unbalanced and operationally unstable above a certain (small) level of heat load fluctuation. The connection between the helium R/L primary circuit and the application system in the secondary circuit is made through the cryo-distribution system, which also helps to smoothen the application load fluctuations. The helium R/L system produces the cryogenic helium at 4 K which is required for various applications in the fusion devices.

The modern helium R/L operates on the modified Claude's cycle with an optimized arrangement of components in order to achieve high efficiency and operational reliability. The high-pressure helium gas from the warm compressor enters the series of heat exchangers before expanding (ideally isentropic expansion) through the turbo expander which extracts energy from the helium and provides a cooling effect. At the final stage of helium R/L, the cryogenically cooled (high pressure) helium expands (isenthalpic expansion) through the Joule-Thompson (J-T) valve in the phase separator and produces liquid helium (LHe). The returning vapor from the phase separator cools the helium gas in counter flow heat exchangers and attains a room temperature before re-entering the warm

[1] Adopted from the article published in Matter Radiation at Extremes, Volume 1, Issue 4, Y. Xu, A general comparison between tokamak and stellarator plasmas, 192–200, Copyright Elsevier (CC BY-NC-ND 4.0 [https://creativecommons.org/licenses/by-nc-nd/4.0/]) (2016).

Table 1. Major parameters of SC tokamak and stellarator worldwide.

	ITER[1] [6, 10, 11]	JT60SA[2] [12, 13]	KSTAR[3] [14, 15, 16, 17]	EAST[4] [18, 19, 20]	SST-1[5] [21, 22]	W7-X[6] [23, 24, 25]	LHD[7] [26, 27]
Cryogenic plant capacity (kW) at 4 K	75	9	9	2[#]	1.3	7	10
Cryogenic plant capacity (kW) at 80 K	1300	68	21[$]	13	NA	9[$]	20
Helium inventory (tons)	27	1.1	1.4	NA	0.6	NA	NA
Cooling mass (tons)	~10000	100	300	169	35	456	850
Cooling principle	forced flow	forced flow	forced flow	forced flow	forced flow	forced flow	forced flow/pool boiling
Flow requirements (kg/s)	3	0.8	0.3	0.32	0.3	0.4	NA
Toroidal field (T) on axis	5.3	2.3	3.5	3.5	3	3	3
Plasma current (MA)	15	5.5	2	1	0.22		
Major radius (m)	6.2	3	1.8	1.7	1.1	5.5	3.5
Minor radius (m)	2	1.18	0.5	0.4	0.2	0.53	.6
Aspect ratio	3.1	2.54	3.6	4.25	5	10.38	5.8
Plasma volume (m^3)	840	140	17.8	11	16	30	32.5
Plasma elongation	<1.8	<2.0	2	1.6–2	<2	NA	NA
Plasma triangularity	<0.5	<0.5	0.8	0.6–0.8	0.4–0.7	NA	NA
Inductive pulse time (s)	>400	100	300	1000	1000	NA	NA

[$] - Thermal intercept at 55 K instead of 80 K.

[#] - Cryogenic plant capacity at 3.8 K instead of 4 K.

[1] ITER is an experimental tokamak being built at Cadarache, France to demonstrate the feasibility of fusion power.

[2] JT60SA is a fusion experiment device under construction/integrated commissioning at Tokai, Japan to investigate the better ways to optimize fusion power plant operations.

[3] KSTAR (Korean Superconducting Tokamak Advanced Research) is a tokamak based nuclear fusion device, under operation at South Korea. It is a step towards the construction of fusion power plant.

[4] EAST (Experimental Advanced Superconducting Tokamak) is designed for fundamental research on tokamak fusion device with a steady, safe and high-performance base for experimental reactor design and construction. It is under operation at Hefei, China.

[5] SST (Steady State Superconducting Tokamak) is a plasma confinement experimental device under commissioning in India.

[6] The Wendelstein 7-X (W7-X) is an experimental stellarator to evaluate the main components of a future fusion power plant commissioned in 2017 at Greifswald, Germany.

[7] Large Helical Device (LHD) is a fusion research device to conduct fusion plasma confinement experiments under operation at Toki, Gifu, Japan.

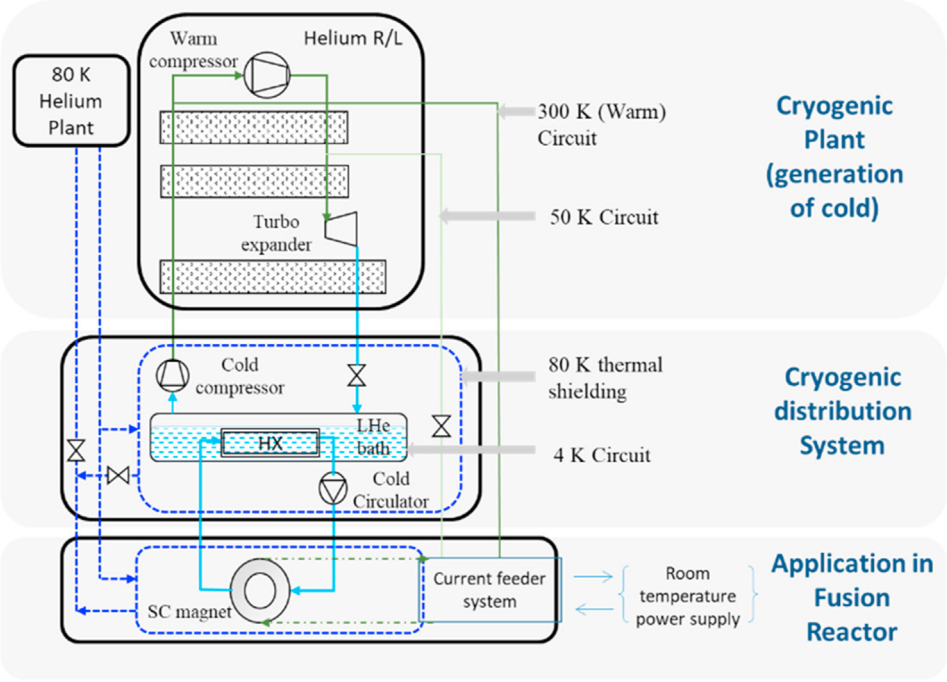

Figure 4. Typical cryogenic cooling Configuration.

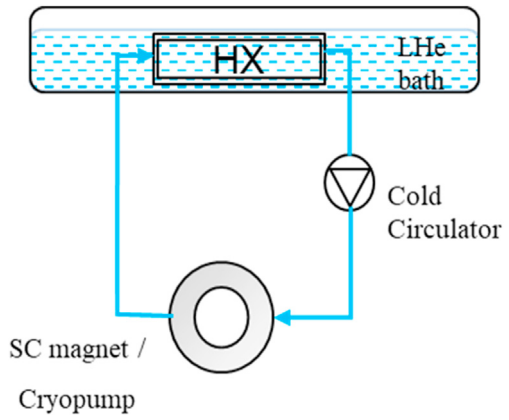

Figure 5. Generalized scheme of forced flow cryogenic cooling.

compressor. The helium R/L thus produces the refrigeration effect through mechanical work and the heat is transferred from source to the sink in a closed circuit (primary circuit). A cold compressor may be used to further reduce the phase separator pressure and hence the LHe temperature, depending upon the requirement. A phase separator or LHe bath maintains the liquid helium through the helium R/L and acts as a cold source for the application. With the help of cold circulator, the flow is maintained in the secondary circuit which connects the application system and the HX inside the LHe bath. The heat from the application system (source) is thus transferred to the LHe in the bath (sink) through the HX in a closed circuit (secondary circuit).

One of the key requirements for the cryogenic system in fusion machines is the removal of large, pulsed heat loads deposited in the magnet system due to the magnetic field variation and neutron production as a result of fusion reaction. The pulsed heat load in fusion device is more relevant for the tokamak based magnetic confinement fusion devices since the current in the plasma is induced by the current swing in a central solenoid, which also induces eddy currents (and hence heat load) in SC Magnets. Broadly, two methods are being utilized for smoothening of pulsed heat load, viz., the application of thermal damper using a sizable LHe bath with buffer volume [12] and/or utilizing the thermal inertia of the huge mass of SC magnet structure [32, 33, 34]. The peak heat load is temporarily absorbed in the thermal damper (in the first case) and then released to the low-pressure side of helium R/L during the dwell period. Whereas in the latter case, the cooling power to the huge magnet structure is reduced during the peak heat load conditions utilizing its thermal inertia without affecting the SC magnet temperature margin, and the magnet structure is cooled again to its initial conditions during dwell time. The helium R/L works in a quasi-steady state condition and produces cold power, whereas the distribution system works in dynamic conditions and removes heat from the application, i.e., superconducting magnets or cryopumps, by forced flow of cold helium as per the requirements of the application.

There can be various arrangements for the cryogenic system in fusion devices, however, the type of arrangement shown in Figure 4 has the main advantage of providing flexibility during the operations in terms of mass flow, temperature and pressure head variation.

The cryogenic application in fusion devices is not limited only to the SC magnets but is also utilized for creating a high vacuum using cryopumps [35], as well as for the cooling of current leads [36, 37] and thermal radiation shield [38]. Cryopumps operate to induce a high vacuum (of the order of 1×10^{-4} Pa) in the cryostat to provide an insulation to the SC magnets and in the vacuum vessel by pumping out air and other impurities at relatively high pumping speed. In yet another application, the cooling of current leads, which provide the bridge between the power supply at room temperature and SC magnets at cryogenic temperature is performed by the cryogenic system. In order to reduce the thermal radiation heat loads from the ambient to the

Table 2. The convective heat transfer correlations for internal flow [52, 53, 54].

Reference	Correlation	Remarks
Kays et al. [51]	$Nu = 3.657 + \frac{0.0668Gz}{1 + 0.04Gz^{\frac{2}{3}}}$	Applicable for thermal entrance region and combined fully developed laminar flow For $Pr > 5$
Kakac, Shah and Aung [55]	$jH = 0.023Re^{-0.2}B_1$ $B_1 = 1$ *for gases* $B_1 = 1.174\left(\frac{\mu_{ave}}{\mu_w}\right)^{0.14}$	for $Re > 3500$;
Dittus Boelter [56]	$Nu = 0.023Re^{\frac{4}{5}}Pr^n$	$n = 0.4$ *for heating of fluid* $n = 0.3$*for cooling of fluid*
Sieder and Tate [57]	$Nu = 0.027Re^{\left(\frac{4}{5}\right)}\ Pr^{\frac{1}{3}}\left(\frac{\mu}{\mu_w}\right)^{0.14}$	Recommended where the fluid property variations is large. For, $0.7 \leq Pr \leq 16700$ $Re \geq 10000$ $\frac{L}{D} \geq 10$
Gnielinski [58]	$Nu = \frac{\left(\frac{f}{8}\right)[Re - 1000]Pr}{1 + 12.7\left(\frac{f}{8}\right)^{\frac{1}{2}}\left(Pr^{\frac{2}{3}} - 1\right)}$	Takes friction factor into account For $3000 < Re < 5 \times 10^6$ For $0.5 < Pr < 2000$
Petukhov [59]	$Nu = \frac{\left(\frac{f}{8}\right)Re\ Pr}{1.07 + 12.7\left(\frac{f}{8}\right)^{\frac{1}{2}}\left(Pr^{\frac{2}{3}} - 1\right)}\left(\frac{\mu_{ave}}{\mu_w}\right)^n$	n = 0.11 for heating n = 0.25 for cooling n = 0 for constant heat flux or for gases For, $0.5 \leq Pr \leq 2000$ (10% *accuracy*) $10^4 < Re < 5 \times 10^6$ $0.8 < \mu_{ave}/\mu_w < 40$
Hausen [60]	$Nu = 3.66 + \frac{0.0668\left(\frac{D}{L}\right)Re\ Pr}{1 + 0.04\left[\left(\frac{D}{L}\right)Re\ Pr\right]^{\frac{2}{3}}}$	Fully developed laminar flow with constant wall temperature. For, Re < 2300 Pr > 5

components at 4 K temperature level, a thermal shield at an intermediate temperature (usually at 80 K) is placed in between the ambient temperature and the 4 K temperature components. The 80 K system for thermal shields is an auxiliary arrangement utilized for efficient cooling in the cryogenic cooling system.

6. Cryogenic fluid flow and heat transfer in fusion device

The cryogenic cooling of the application system in a fusion device effectively utilizes the Forced Flow Cooling (FFC) (see Figure 5) in complex geometries to remove the static and transient thermal loads.

The forced flow cryogenic cooling of SC magnets and cryo-adsorption pumping panels in fusion devices are challenging due to the intricate geometries of fluid flow channels coupled with the impingement of heat flux in various modes such as convection, solid and gas conduction, thermal radiation, electrical energy dissipation within the conductor and ionizing radiation. The cryogenic fluid flow is hydraulically characterized by fluid flow conditions and flow passage geometry such as simple conduit, annular space, porous medium, bubble plates, external or internal flow in plates.

The complete description in a mathematical model to capture the forced flow cryogenic cooling in time and space involves the following form of mass conservation, momentum conservation and energy conservation:

$$\frac{\partial \rho}{\partial t} + \nabla.(\rho \boldsymbol{V}) = 0 \qquad \text{Eq. 2}$$

$$\frac{\partial(\rho u)}{\partial t} + \nabla.(\rho u \boldsymbol{V}) = -\frac{\partial p}{\partial x} + \frac{\partial \tau_{xx}}{\partial x} + \frac{\partial \tau_{yx}}{\partial y} + \frac{\partial \tau_{zx}}{\partial z} + \rho f_x \text{ [x direction]} \qquad \text{Eq. 3}$$

$$\frac{\partial(\rho i)}{\partial t} + \nabla(\rho i \boldsymbol{V}) = -\nabla.(p \boldsymbol{V}) + \nabla.(k\, \boldsymbol{grad}\, T) + S_E + V_E \qquad \text{Eq. 4}$$

The numerical modelling and simulation (or system-level simulation) enveloping the thermal, hydraulic, electromagnetic and geometrical aspects is a useful tool to capture the entire domain associated with the cryogenic cooling, however, the semi-empirical data such as the friction factor and the heat transfer coefficients, are required to support the system-level simulation.

The VINCENTA [39] simulation model couples the 1-D thermo-hydraulic model for the SC cables and 2-D thermal diffusion model for the transverse heat conduction at a few discrete locations. The 1-D model is used to simulate the transient behavior of compressible helium flow in CICC while the 2-D heat diffusion model is used to simulate the heat diffusion in the support structure. This model can simulate the whole coil with its cryogenic loop, leading to a detailed but complex model. The validation of the VINCENTA model has been done

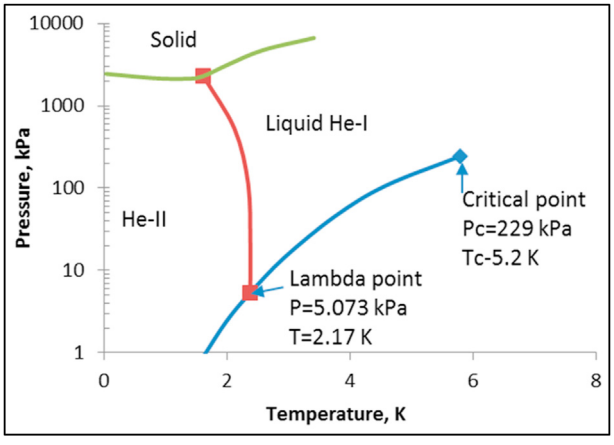

Figure 6. The phase diagram of Helium-4.

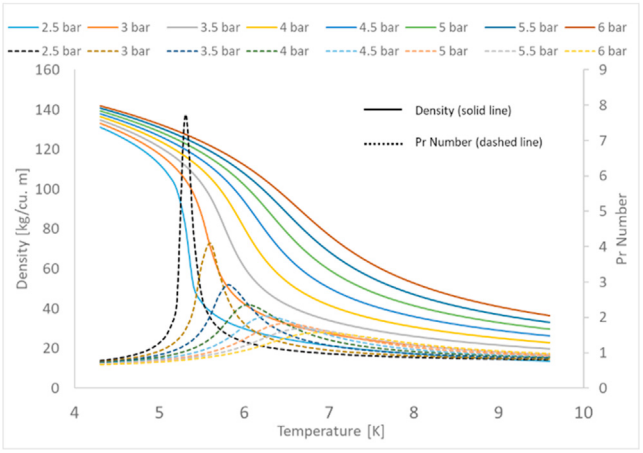

Figure 7. Fluid property variations near to critical point for Helium.

for CSMC of ITER [39]. Also the simulation of the ITER TF coil has been performed with the VINCENTA model [40] which is also a basis for the specification of the cryogenic forced flow cooling loop of ITER [32].

The SuperMagnet [41] model uses the existing tools and joins them in a customizable and flexible way to simulate the thermo-hydraulic and electrical transients in the SC magnets including the cryogenic circuit and power supply [41]. It is composed of a FLOWER module for the hydraulic network simulation, a THEA module for Thermal, Hydraulic, and Electric Analysis of the SC cables, a POWER module for the electrical network simulation, and a HEATER module for the simulation of the transverse heat conduction. The SuperMagnet is a manager that launches two or more of above-mentioned code for their execution. The code has been validated for the 15 MA scenario operation against the VINCENTA code [41].

The Cryogenic Circuit Conductor and Coil (4C) code [42] allows the thermo-hydraulic transient simulation of the entire SC magnet system and in particular the CICC windings, the structures (radial plate and casing) and the cooling circuits. The code combines different components and integrates them in a single tool. The 4C code has also been validated against the experimental data of W7-X for the cool-down from room temperature to the SC transition temperature ~10K [43]. The thermo-hydraulic validation of the code has also done for the 25kA safety discharge of the TFMC [44]. The 4C code has been rigorously validated for various SC magnet system [43, 44, 45, 46, 47, 48, 49] including even predictive validation where the simulations are performed before/without the knowledge of the results of the measurements [50]. The rigorous validation activity carried out on 4C code puts it in a different perspective with respect to the others.

6.1. Convective heat transfer studies in helium

The convective heat transfer studies for internal flows, i.e., through the circular pipe, has been widely [51] conducted and several convective heat transfer correlations are available in the published literature [52, 53, 54]. The major convective heat transfer correlations are listed in Table 2.

The convective heat transfer studies for helium fluid is, however, of particular interest for the fusion devices due to the exclusive use of helium to achieve a low temperature of the order 4 K. The basic requirement of heat transfer studies is the knowledge of thermodynamic and transport properties of the fluid (helium), which are available through NIST database (https://webbook.nist.gov) [61] for a wide range of pressure and temperature conditions. Helium has specific properties as compared to other fluids [62], as its critical point is not so far from the saturated liquid point at atmospheric pressure and it becomes a superfluid (He-II) at lambda point (as shown in Figure 6 which is drawn schematically based on the data from NIST database).

Table 3. The heat transfer coefficients for internal flow of helium (in Eq. 5).

Reference	Coefficient C_1 to C_4 in Eq.					Remarks
	C_1	C_2	C_3	C_4	σ	
Dittus-Boelter	0.023	0.8	0.4	0	10–20%	
Giarratano et al. [64, 70]	0.0259	0.8	0.4	-0.716	8.5%	C_1 *to* C_4 shown above are with least σ
Giarratano et al. [64, 70]	0.0258	0.801	0.461	-0.711	8.3%	
Pron'ko et al. [65, 71]	0.036	0.8	1.2	0		
Brassington et al. [67, 68] Upward flow	0.0602	0.718	0.5	-0.48	8.5%	Pr is harmonic average over the range T_w *and* T_b
Brassington et al. [67, 68] Downward flow	0.0931	0.687	0.53	0	6.4%	

A summary of heat transfer in helium-I for various regions of the helium phase diagram is presented by R. V. Smith [63]. The various regions of helium phase diagram are mainly divided into four zones (i) the pool boiling region under the liquid-vapor dome of the helium, (ii) the region near the critical point and transposed or pseudo critical line, (iii) the supercritical helium liquid-like region and (iv) the supercritical helium gaseous like region.

The helium properties largely vary near the critical point and near the transposed critical line. The variation of density and Prandtl number at various pressures (isobars) has been shown in Figure 7 based on the NIST fluid properties data for helium. The various heat transfer studies for supercritical helium heat transfer have been carried out [64, 65, 66, 67, 68, 69] for the internal flow and most of the correlations were suggested based on the Dittus Boelter correlation as given in a general form in Eq. (5).

$$Nu = C_1 Re^{C_2} Pr^{C_3} \left(\frac{T_w}{T_b}\right)^{C_4} \quad \text{Eq. 5}$$

Where C_1 *to* C_4 are different coefficients suggested to best fit the experimental results with the least standard deviation. The fluid property variation near the pseudo or transposed critical line is taken care of by the property ratios at wall temperature and bulk fluid temperature. The coefficient C_1 *to* C_4 in Eq. (5) as obtained by various researchers are tabulated in Table 3.

The above empirical correlations are for the simple circular conduit. The hydraulic diameter for the cross-section and length represent the required geometric information for fluid flow and heat transfer correlations.

6.2. Thermo-hydraulic studies in CICC

The review of fluid flow and heat transfer studies for helium fluid is further extended for the special cases utilized in the fusion devices such as SC magnets made from the winding of special cable called Cable in Conduit Conductor (CICC). The CICCs are made from tiny multi-filamentary wires made of superconducting material such as NbTi or Nb_3Sn with a mixture of normal conductor, like copper, as a stabilizing agent. The SC strands are paired and twisted to make a cable, e.g., twisting of strands in a pattern 3x3x4x5x6 to make a cable with 1080 strands. The cables are encased in a jacket, made of stainless steel or aluminum, to provide mechanical strength. The cryogenic cooling fluid passes through the voids between the SC strands. Sometimes relief hole(s) is provided as the coolant passages. There have been several improvements in the design and construction of CICC since it was first proposed by Hoenig and Montgomery in 1970s [72]. The typical cross-sections of such Cable in Conduit Conductor (CICC) are shown in Figure 8 in which Type (a) CICC used in SST-1 [73], Type (b) CICC used for W7-X [74], Type (e) CICC used for ITER PF and CS conductor samples [75, 76], Type (g) CICC used for TF conductor sample for the ITER project [77] and Type (h) CICC is ENEA conductor envisaged for the EU DEMO [44].

CICC functions as electrical conductors for SC magnet and is continuously cooled, through channel(s) provided for the coolant, by helium at 4 K temperature to remain a superconductor. In the context of SC magnets, the coolant must overcome the a.c. losses, neutron heat flux, thermal radiation and solid conduction heat load during the magnetically confined fusion process. Studies related to the fluid flow and heat transfer through the complex geometry of the CICC are therefore necessary to predict the conductor cooling, magnet quench behavior and to ensure the stability as well as effective cold source requirement at 4 K temperature.

Katheder [78] proposed, in 1994, the optimum operating regime for CICC from the first principles and suggested that for a typical CICC geometry, the optimum pressure should be between 6 and 7 bar. The study also proposed friction factor for Type-(a), (b) and (c) CICC based on a standard formula used for pebble beds, which takes into account the void fraction in the CICC. Katheder's work is pioneering for CICC thermo-hydraulic studies and has been referred subsequently by other researchers. The thermo-hydraulic characteristics of Type-(a) CICC was analyzed for Wendelstein 7-X magnet, in 1994, by X. Cheng et al. [74, 79] and proposed friction factor with an empirical coefficient from the experimental data. The evaluated pressure drop was found to be 3 times higher than that for an equivalent smooth tube. However, the proposed correlation of friction factor did not mention the effect of void fraction, which is an important parameter for the pressure drop. In the same experimental set-up [79], the transverse heat transfer coefficient was proposed which is a modified form of Dittus-Boelter correlation.

S. Nicollet et al., in 1998, proposed a friction factor correlation for ITER TFMC CICC, Type-(g), a bundle region as derived from Katheder formulae but with different parameters [80]. This correlation takes into account the void fraction and the Reynolds number. S. Nicollet et al. proposed, in 2000 [77,81], a friction factor correlation for the central hole region delimited by central spirals. The correlations depend on the type of the central spiral and their characteristics, specially, the twist pitch length and the turn length. R. Zanino et al., in 2000 [82], proposed another approach, based on an equivalent roughness of the central relief hole, to determine the friction factor correlation for the central hole region.

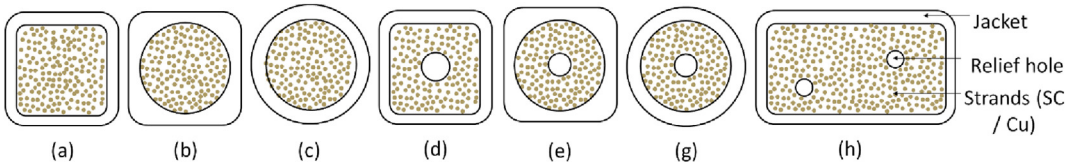

Figure 8. Various typical cross-sections of CICC [(a) square jacket without relief hole (b) internally round jacket without relief hole (c) round jacket without relief hole (d) square jacket with relief hole (e) internally round jacket with relief hole (g) round jacket with relief hole (h) rectangular jacket with two relief holes].

Table 4. A summary of experiments conducted for studying the pressure drop in CICC.

	CICC Sample	W7-X	TFMC	ITER CS1	PFCI	PFCI	COND OPT-1	COND OPT-5	TFC for EU Demo
	Year	1994	2000	2001	2005	2005	2008	2008	2018
	Reference	[74]	[77]	[76, 97]	[75]	[75]	[96]	[96]	[44]
Geometrical data	Type (refer Figure 8)	(b)	(g)	(e)	(e)#	(e)&	(g)	(g)	(h)
	SC strand	NbTi	Nb3Sn	Nb3Sn	NbTi	NbTi	NbTi	NbTi	Nb3Sn
	SC strand dia (mm)	0.55	0.81	0.81	0.73	0.73	0.87	0.7	1
	Cu strand dia (mm)	NA	NA	NA	NA	NA	0.62	0.7	1.5
	No. of SC strands	192	720	1152	1440	1440	48	48	1080
	No. of Cu strands	NA	360	NA	NA	NA	336	288	132
	Total no. of strands	192	1080	1152	1440	1440	384	336	1212
	Cos θ	NA	NA	0.925	0.96	0.96	0.985	0.981	0.95
	Length (m)	1.36	72.2	1	1	0.631	3	3	2.546
	Jacket inner dimension (mm)	9.4	37.5	38.99	37.53	36.89	15.5	15.5	66.6 × 25
	OD of relief hole (mm)	NA	12	11.8	12	12	NA	NA	6.6
	ID of relief hole (mm)	NA	10	9.8	NA	NA	NA	NA	4.6
	Total strand c/s (mm2)	45.6@	579.11	642	627.808	627.808	131	133.7	1081.5@
	Total cable space (mm2)	69.1@	1097.2	1194	1106.234	1068.827	188.6	188.7	1665.0@
	Flow area bundle (mm2)	23.5@	355.2	396	332.429	327.921	50.4	47.7	378.6
	Flow area relief (mm2)	NA	113.09	76	113.097	113.097	NA	NA	33.24
	Void fraction	0.34	0.3685	0.365	0.33473	0.34311	0.267	0.249	0.246
	Wetted perimeter (mm)	361.2@	3193	3610	3222.983	2886.166	504	459	4239.6@
	Hydraulic dia bundle (mm)	0.3	0.445	0.438	0.413	0.454	0.399	0.416	0.336
Experimental conditions	Fluid	Helium	Nitrogen	Water	Water	Water	Water	Water	SHe
	Temp. (K)	5–20 K	293	301	299	300	room	room	4.5–13 K
	Inlet pressure (MPa)	0.3–0.7	0.2–0.67	1.1	0.8	0.8	0.1	0.1	1
	Mass flow rate range (g/s)	0.3–2.5	127.5	0–800	0–800	0–800	0–80	0–60	1–10
	Reynolds number (bundled region)	1000–10000	8000–9000	10–1000	1117	1244	712	784	10–2000

& - without cable wrap.
# - with cable wrapss
@ - calculated value.

ITER Central Solenoid Model Coil (CSMC) test results were presented by K. Hamada et al. [76], in 2002. CSMC utilize Type-(e) conductor and therefore two different pressure drop correlations were applied, one for the bundled region and the other for the relief hole region as per ITER design criteria. R. Zanino et al. [83], in 2006, proposed to utilize the porous media analogy approach for the CICC bundled region. Claudio Marinucci et al. [84] proposed, in 2007, an approximate analysis to obtain the mass flow rates in a bundled region to predict the friction factor coefficient and concluded the friction factor to be 0.7 times the value obtained by Katheder's [78] correlation. M. Bagnasco et al. [85], in 2010, proposed friction factor correlation and M. Lewandowska et al. [86], in 2011, proposed a modified friction factor based on the porous media analogy.

S. Nicollet et al. [87], in 2004, proposed a convective heat transfer coefficient based on steady state helium measurements temperature along heated and non-heated zone of a short length of CICC, and also laws for transverse heat transfer coefficient in CICC between bundle region and central hole region. The mass and heat transfer between the central channel and bundle region were studied with mass and energy balance method by Zanino et al. [83], in 2006. L. Bottura et al. [88] proposed, in 2006, transverse heat transfer coefficient for CICC with relief hole Type-(c). The study further distinguished the bundle region; strands wrapped with a steel band and without steel wrap. The method was based on the temperature measurement in time and space during a pulsed heat load condition. The term 'effective thermal conductivity k_{eff}' was proposed by Claudio Marinucci et al. [84], in 2007, related to ITER CICC, Type-(c). The flow distribution and heat transfer coefficient between the central channel and the bundle region in the ITER TF conductor was determined based on a direct heat and mass transfer analysis of the temperature measurements at steady state.

The difficulties of scaling up the model from a small geometry scale to a bigger scale of a few hundred meters length of CICC were discussed for fusion grade machines [83]. A CFD based numerical analysis approach for the central relief hole [89, 90] and a friction factor correlation deduced from the CFD analysis of CICC was proposed by Zanino et al. [91] in 2006. A CFD based analysis approach was adopted and reported by Sekhar [92, 93, 94, 95] by developing a 3D model to estimate the pressure drop and heat transfer in CICC considering it as a partially filled porous medium for bundled region [92]. It was also reported that the thermal gradients develop due to transport of turbulence through CICC even without external heat sources [93] and the turbulence in the flow causes the occurrence of recirculation zones at leading and trailing edges of the central spiral rib thereby initiating formation of eddies [94].

Dedicated thermo-hydraulic tests were carried out for Type-(h) CICC on a full scale, short length CICC sample having a rectangular cross-section with two small pressure relief 'holes' of 5 mm diameter [44]. The CICC consisted of Nb_3Sn strands with copper as a stabilizer for TF magnet cooled by SHe. The test results obtained from the actual test as well as from the CFD simulation for the hole were compared with the proposed friction factor correlation [86] and utilized to calibrate the developed numerical code [98].

A summary of experiments carried out for pressure drop measurement and predicting the friction factor is given in Table 4. The proposed friction factor coefficient and heat transfer correlations by various researchers are summarized in Table 5 and Table 6 respectively.

As observed from Table 5, the friction factor has been described as a function of one or more parameters such as Reynolds number, void fraction and hydraulic diameter for the bundled region. However, the cabling pattern and surface roughness of strands/jacket is not considered as a parameter in any of the studies.

For an identical CICC geometry, the variation of friction factor as a function of Reynolds number (in the range of 100–10000) and a void fraction (20%, 30% and 40%) is shown in Figure 9. The Darcy friction factor for laminar flow as well as the Haaland friction factor for turbulent pipe flow have also been considered for comparison with available correlations for the friction factor in CICC. The difference between the

Table 5. A summary of studies related to friction factor coefficients.

Reference	Friction factor	Remarks	Type of CICC	Nomenclature
X. Cheng [74, 79]	$\frac{1}{\sqrt{f}} = 0.87\ln(R_e\sqrt{f}) - A$	Proposed coefficient, A = 3.3 based on experiment. Reported measurement; ~2000 < Re < ~10000	(b)	f = *Darcy friction factor* A = *Area* f_a = *void fraction in budled region* p = *wetted perimeter* ρ = *fluid density* C_F = *Drag coefficient* R_e = *Reynolds number* P_r = *Prandtl number* d = *hydraulic diameter* K = *Permeability* β_0 = *Coefficient* $C_F/\sqrt{K}$
H. Katheder [78]	$f = \frac{1}{f_a^{0.72}}\left[\frac{19.5}{Re^{0.88}} + 0.051\right]$	Correlation has been proposed based on pebble bed analogy 8000 < Re < 17000	(a) (b) (c)	
S. Nicollet [77, 80, 81, 82]	$f = \frac{1}{f_a^{0.72}}\left[\frac{19.5}{Re^{0.7953}} + 0.023\right]$ For relief hole region; $f = 0.3024\,Re^{-0.0707}$ Showa Spiral $f = 0.7391\,Re^{-0.1083}$ Cortaillod Spiral	Correlation based on Katheder formulae but with different parameters 1000 < Re < 6000 Correlation for relief hole with two different delimiter central spirals, (i) Showa (ii) Cortaillod. Reported measurement; ~10000 < Re < ~500000		
K. Hamada et al. [76]	For bundled region; $f = \frac{1}{f_a^{0.72}}\left[\frac{19.5}{Re^{0.88}} + 0.051\right]$ For relief hole region; $f = 0.046\,N\frac{1}{Re^{0.2}}$	Correlation is the same as proposed by Katheder [78] for the bundled region Correlation for relief hole region with a recommended value of Coefficient N = 2 to 7 10000 < Re < 100000	(e)	
Claudio Marinucci et al. [84]	For bundled region; $f = 0.7\,\frac{1}{f_a^{0.72}}\left[\frac{19.5}{Re^{0.88}} + 0.051\right]$	Proposed friction factor is 0.7 times the friction factor proposed by Katheder [78] 10 < Re < 1000 for bundled region	(e)	
M. Lewandowska and M. Bagnasco [86]	$f = \frac{d^2 f_a}{2K}\frac{1}{Re} + \frac{d f_a^2}{2}\frac{\beta_0}{f_a^{4.23}}\left(\frac{d}{f_a Re\sqrt{K}}\right)^{0.14}$ $\beta_0 = 19.1$ (*for non − braided CICC*) $\beta_0 = 41.9$ (*for braided CICC*) $K = 20.9\cdot 10^{-19}\frac{f_a^3}{(1-f_a)^2}$	Correlation has been proposed based on analogy with porous media 100 < Re < 100000	(d) (e) (g)	

Table 6. A summary of studies related to heat transfer correlations.

Reference	Heat transfer coefficient	Remarks	Type of CICC	Nomenclature
X. Cheng [74, 79]	$Nu = (1 - f_a)Nu_0 + f_a\, Nu_1$ $Nu = 0.53(17.5 + 0.023Re^{0.8}Pr^{0.4})$	Transverse heat transfer from jacket to fluid and Jacket to strands. Recommended value from the experiment. $f_a = 0.53$ $Nu_0 = 19.7$	(b)	Nu = *Nusselt number* k = *thermal conductivity* v = *velocity of flow* h = *heat trasnfer coefficient*
L. Bottura [88]	$k = \frac{A_H^2 - A_B^2}{(A_H + A_B)^3}\left(\frac{\rho C_p}{p\,h}\right)(v_H - v_B)^2$	Heat transfer between bundle to relief hole region. Transient temperature measurement method.	(e)	C_p = *specific heat of fluid* k = *thermal conductivity* *subscript;* B = *bundled region* H = *central hole regio*
S. Nicollet [87]	$h = f\,\frac{2}{8}\frac{k\,Re\,Pr^{\frac{1}{3}}}{d}$	Heat transfer coefficient for bundled region.	(e)	
Claudio Marinucci et al. [84]	$h = 0.023\,Re^{0.8}Pr^{0.4}\frac{k_{eff}}{d}$	Heat transfer coefficient for bundled region.	(e)	
M. Lewandowska and L. Malinowski [98]	$Nu = CRe^{n}Pr^{\frac{1}{3}}$	Coefficient for bundled region. C and n proposed from the experiment	(e)	

various proposed friction factor increases with an increase in void fraction and decreases at high Reynolds number. The friction factor proposed by X. Cheng [74] is independent of the void fraction and hence there is no variation for different void fractions.

6.3. Thermo-hydraulic studies in cryopump panels

Yet another application of forced flow cooling in fusion devices is the cryo-adsorption pumps which are used to pump down unwanted gases for nuclear fusion to take place and to maintain the required vacuum in the torus. The major sources of heat load in a cryopump cooling panel include thermal radiation, solid conduction, gas conduction and energy transfer from the pumped gas.

The geometry of cryo-adsorption panels is designed to maximize the heat transfer area and minimize the flow losses within the given space constraints. The usual geometry is a hydraulically formed dimple panel (HFDP) in which fluid is passed through the flow passages which are created between two spot-welded (in a certain pattern) flat metallic sheets by inflation. The HFDP for cryopump application is a widely accepted solution as a heat transfer device for many other industrial applications too, e.g., thermal shield, heat jacket etc. A typical cooling panel for cryopump is shown in Figure 10. For the effective pumping of helium and hydrogen gases from the torus, the HFDPs are coated with an adsorption material. Several developments have been made to effectively characterize the pumping speed of cryopump with various adsorption materials [99, 100, 101, 102].

The theoretical estimation of the pressure drop through a typical HFDP needs information of the flow cross-section (circular segment) as shown in Figure 10, where a is the sag, R is the radius, θ is the central angle and c is the chord of the circular segment. The flow cross-section A_{flow} and the wetted perimeter p for one circular segment of HFDP are given by

$$A_{flow} = 2 \cdot \frac{R^2}{2}(\theta - \sin\theta) \quad \text{Eq. 6}$$

$$p = 2R\theta \quad \text{Eq. 7}$$

$$d = 4\frac{A_{flow}}{p} \quad \text{Eq. 8}$$

The pressure drop ΔP can be expressed in terms of the hydraulic diameter d, an equivalent characteristic length L_{eq}, an effective flow area A_{flow} and the mass flow through the panel [103].

$$\Delta P = \zeta\frac{\rho L_{eq} v^2}{2d} = \zeta\frac{L_{eq}\dot{m}^2}{2\rho A_{flow}^2\, d} \quad \text{Eq. 9}$$

The hydraulic diameter, d, is defined at the HFDP mid cross-section. The pressure loss coefficient ζ is a function of Reynolds number Re and other geometric characteristics.

The complex geometry of the HFDP does not allow simple analytical formulae to be applied for the fluid flow and heat transfer analysis as the theoretical estimation of hydraulic diameter, characteristics length and fluid-solid interaction is difficult for such a geometry. The pressure loss coefficient is highly dependent on the flow pattern made on HFDP and hence the experimental and numerical validation is necessary for the thermo-hydraulic characterization.

Scannapiego et al. [103] carried out experimental and numerical investigation for pressure drop at different mass flow rates (0.5–3.5 kg/s) and obtained a good agreement between the two results. The largest plate central region contributes only up to <50 % of the overall pressure drop, whereas the sudden enlargement/restriction in cross-sectional area between the inlet/outlet piping and the plate, and the resulting diverging/converging flows result in large pressure losses.

Suhagiya et al. [104] carried out analytical calculation as well as numerical investigation using ANSYS® for heat transfer and pressure

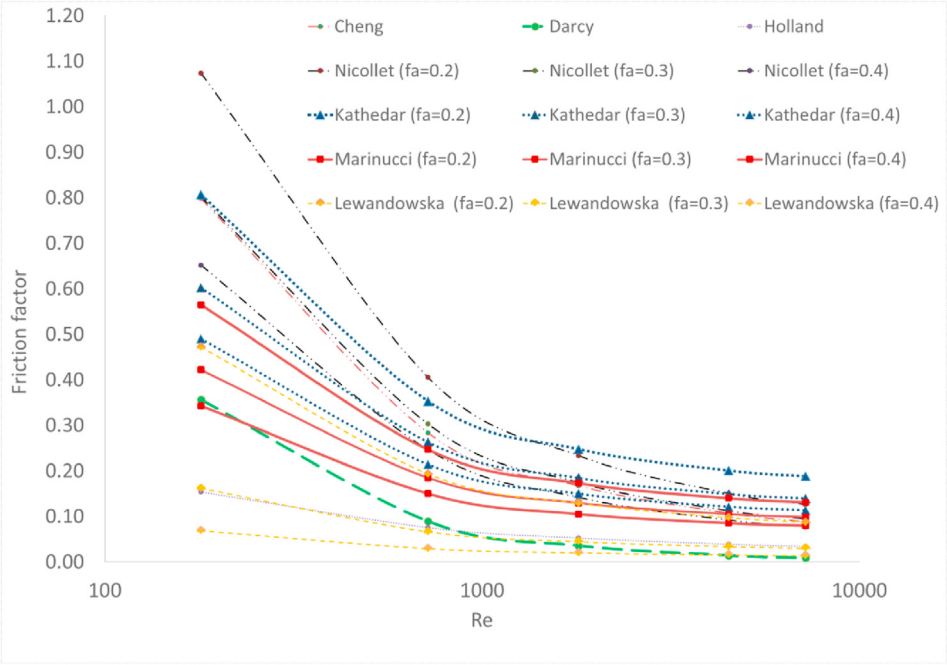

Figure 9. The variation of friction factor as a function of Reynolds number with different void fractions (f_a) based on various correlations.

drop for a single panel of a cryopump. The variation of 2%, 18.6% and 0.7% are found for the pressure drop, velocity and surface temperature respectively between analytical and numerical calculations.

Copra et al. [105] numerically analyzed two different cases based on the arrangements of inlet and outlet ports. The favorable arrangement (i.e., two inlets at the end and one outlet at the center of the panel) were further investigated for different mass flow rates between 20 g/s to 50 g/s. A maximum pressure drop of 128 mbar was obtained with temperature less than 90K in 95% of the panel area.

Sanghani et al. [106] considered fluid-solid interaction in a numerical computation validated through experiment. The experimental and CFD techniques showed a pressure drop of 3000 Pa and 2311 Pa for the surface temperature of 280.4 K and 280.6 K respectively.

A summary of experimental and computation investigations conducted for the cryo-adsorption pump panels is presented in Table 7.

6.4. Challenges ahead

The forced flow cryogenic cooling of SC magnets and cryo-adsorption pumping panels in fusion devices are challenging due to the intricate geometries of fluid flow channels coupled with an impingement of heat flux in various modes such as convection, solid and gas conduction, thermal radiation, electrical energy dissipation (for the conductor) and ionizing radiation. The thermal stability of SC magnet is achieved through the forced flow cooling while overcoming the various static and pulsed heat loads in any modern fusion device. The design of the SC CICC and cryopump panel are evolving continuously for efficient cryogenic cooling while maintaining their primary functions in an optimized manner. This evolvement makes it more challenging to establish predictive correlations for thermo-hydraulic behavior for CICC and cryopump panels. The following challenges are foreseen in order to make the technology viable in future:

(i) The existing predictive correlations for the bundled region friction factor for CICC is based on analogical correlations, e.g., rough pipe, porous media, pebble bed etc. However, further insight of CICC construction, twisting pattern, relative roughness etc., would improve the prediction of pressure drop.

(ii) It is obvious that CICC with relief hole(s) will reduce the hydraulic impedance in long length and enhance the heat transfer and the global cooling capacity of the fluid through both regions of CICC. Indeed, adding a central cooling channel (and additional mass flow through central hole) reduces the Reynolds number in the bundle region, and thus increase the friction factor and the convective heat exchange coefficient. However, the mass flow distribution and mixing between the bundled region and relief hole is a function of mass flow rate and their individual hydraulic impedance needs to be included in the correlations for friction factor of the bundled region and relief hole(s) in an interlinked manner.

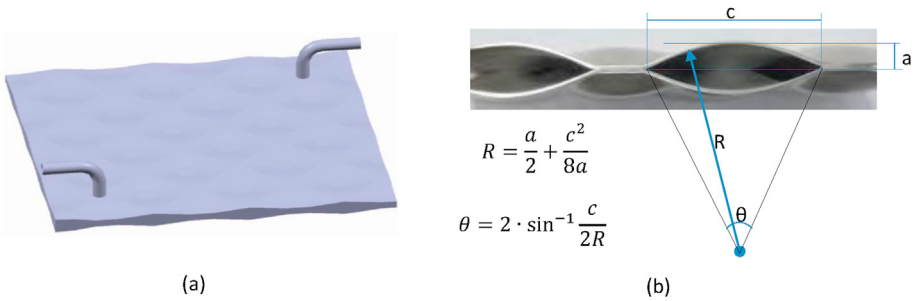

Figure 10. (a) A typical cooling panel for cryopump (b) typical cross-sectional view of the flow area.

Table 7. Review of experimental and computation investigation made for cryo-adsorption pump panels.

Type of Panel	Overall size	Type of investigation	Fluid	Temp. range	Reference
HFDP with diamond pattern spot welds and diagonal input/output.	2.31 m × 0.52 m	Experimental	Water	350 K	[103] Scannapiego et al
HFDP with diamond pattern spot welds and diagonal input/output.	2.31 m × 0.52 m	Numerical	Water GHe	350 K 80 K	[103] Scannapiego et al.
HFDP with spot welded and seam welded lines and diagonal Input/ output.	1 m × 0.2 m	Analytical and numerical	SHe	4.5K	[104] Suhagiya et al.
HFDP with diamond pattern spot welds and having two inlets and one outlet of different configurations.	2.045 m × 1.8 m	Numerical	GHe	80 K	[105] Copra J et al.
HFDP with diamond pattern spot welds and seam welding at edge with diagonal inlet/outlet.	0.5 m × 0.5 m	Numerical and experimental	Chilled Water	280K	[106] Sanghani et al.

(iii) While the HFDP of the cryopumps can be modeled and simulated to study the thermo-hydraulic characteristics using the finite element or numerical techniques, it is difficult to exactly model and simulate the CICC using finite element technique for thermo-hydraulic studies.

(iv) The ultimate goal of the thermo-hydraulic analysis of the CICC is to ensure the SC magnet stability, however, the overall performance prediction of SC magnet from the cross-sectional geometry of CICC is difficult. The SC magnet is formed by winding of CICC of few hundred meters in length with certain curvature, several joints, terminations etc. The thermo-hydraulic study of the CICC cross-section considering a straight length is not sufficient for thermo-hydraulic characterization of the SC magnet. The development of SC magnet simulation codes are helpful to predict or analyze the thermal-hydraulic behavior of SC magnet including the transient conditions such as the quench. Such simulation codes are quasi 3-D due to the computational efforts required to make it full 3-D. With the advancement in high performance computing, further development in simulation and code development is possible.

(v) The hydraulic behavior under the pulsed heat load and internal heat generation (during quench) condition for the fusion grade SC magnets is yet to be studied. More accurate prediction of the CICC thermo-hydraulic performance in the complex construction of the SC magnet will certainly be beneficial to design higher magnetic field SC magnets.

(vi) In the context of cryogenically cooled HFDP for fusion devices, the prediction of more accurate pressure losses and heat transfer coefficient is very important to save energy for the helium R/L. There is a need to establish correlations for pressure loss and heat transfer coefficient for the most frequently used HFDP patterns and utilize the same in the numerical simulation to get a complete picture of the fluid and temperature profile.

7. Conclusions

In order to cope with the increasing energy demand, nuclear fusion represents the potential option for providing clean and abundant energy. In the nuclear fusion devices, cryogenic cooling involves the forced flow circulation of helium by CCP in the CICC of the SC magnets as well as in the HFDP of the cryopumps. In the present study, a state-of-the-art review of forced flow cryogenic cooling in nuclear fusion devices is conducted. The fluid flow and heat transfer characteristics specific to the SC magnets and cryopumps in nuclear fusion devices are presented.

The accurate prediction of the CICC thermo-hydraulic performance in the complex construction of the SC magnet will be beneficial to design higher magnetic field SC magnets. The thermo-hydraulic studies carried out for the CICC shows that the correlations for the hydraulic characteristics are mainly proposed based on different analogies such as pebble bed and porous medium without specifying all the geometric details. Similarly, within the CICC, the heat transfer coefficient in the transverse direction has been proposed by various researchers based on modifications of the Dittus Boelter correlation with support from experimental data. In the same line, it is highlighted that the cooling channel for cryopump using HFDP pose similar complexity in thermo-hydraulic prediction as in the case of CICC. The thermo-hydraulic characteristics of the cryopump HFDP have been addressed through a combination of numerical and experimental studies.

Declarations

Author contribution statement

All authors listed have significantly contributed to the development and the writing of this article.

Funding statement

This research did not receive any specific grant from funding agencies in the public, commercial, or not-for-profit sectors.

Data availability statement

No data was used for the research described in the article.

Declaration of interests statement

The authors declare no conflict of interest.

Additional information

No additional information is available for this paper.

Acknowledgements

The authors acknowledge the support received from the Institute for Plasma Research and ITER-India for conducting the present study. We gratefully acknowledge the valuable suggestions and critical comments of reviewers in enhancing the quality of paper.

Disclaimer: The views and opinions expressed herein do not necessarily reflect those of the ITER Organization and the ITER partners.

References

[1] R.E.H. Sims, R.N. Schock, A. Adegbululgbe, J. Fenhann, I. Konstantinaviciute, W. Moomaw, H.B. Nimir, B. Schlamadinger, J. Torres-Martínez, C. Turner, Y. Uchiyama, S.J.V. Vuori, N. Wamukonya, X. Zhang, Climate change 2007 - mitigation of climate change, in: ., Energy Supply. Clim. Chang. 2007 Mitigation. Contrib. Work. Gr. III to Fourth Assess. Rep. Intergov. Panel Clim. Chang, Cambridge University Press, 2007, pp. 253–315. http://www.ipcc.ch/publications_and_data/.

[2] S. Deshpande, P. Kaw, Fusion research programme in India, Sadhana 38 (2013) 839–848.

[3] R. Srinivasan, Role of fusion energy in India, J. Plasma Fusion Res. 9 (2010) 630–634.

[4] G. McCracken, P. Stott, Fusion - the Energy of the Univers, Elsevier, 2005.

[5] M. Kikuchi, A review of fusion and tokamak research towards steady-state operation: a JAEA contribution, Energies 3 (2010) 1741–1789.

[6] https://www.iter.org. (Accessed 24 April 2018).

[7] R. Betti, P.Y. Chang, B.K. Spears, K.S. Anderson, J. Edwards, M. Fatenejad, J.D. Lindl, R.L. McCrory, R. Nora, D. Shvarts, Thermonuclear ignition in inertial confinement fusion and comparison with magnetic confinement, Phys. Plasmas 17 (2010) 1–10.

[8] Y. Xu, A general comparison between tokamak and stellarator plasmas, Matter Radiat. Extrem. 1 (2016) 192–200.

[9] V.P. Smirnov, Tokamak foundation in USSR/Russia 1950-1990, Nucl. Fusion 50 (2010) 1–8.

[10] E. Monneret, M. Chalifour, M. Bonneton, E. Fauve, T. Voigt, S. Badgujar, H.S. Chang, G. Vincent, ITER cryoplant status and economics of the LHe plants, Phys. Procedia. 67 (2015) 35–41.

[11] R. Maekawa, S. Takami, A. Iwamoto, H.S. Chang, A. Forgeas, M. Chalifour, L. Serio, Process analyses of ITER toroidal field structure cooling scheme, Cryogenics 63 (2014) 220–230.

[12] C. Hoa, M. Bon-Mardion, P. Bonnay, P. Charvin, J.N. Cheynel, B. Lagier, F. Michel, L. Monteiro, J.M. Poncet, P. Roussel, B. Rousset, R. Vallcorba-Carbonell, Investigations of pulsed heat loads on a forced flow supercritical helium loop - Part A: experimental set up, Cryogenics 52 (2012) 340–348.

[13] http://www.jt60sa.org/pdfs/cdr/10-3.5_Cryogenic_System.pdf. (Accessed 19 March 2017).

[14] C.H. Choi, H.S. Chang, D.S. Park, Y.S. Kim, J.S. Bak, G.S. Lee, I.K. Kwon, H.M. Kim, M.C. Cho, H.S. Kim, E. Fauve, I. Abe, P. Briend, J.M. Bernhardt, Y. Cardet, P. Dauguet, J. Beauvisage, F. Andrieu, S.H. Yang, G.M. Gistau Baguer, Helium refrigeration system for the KSTAR, Fusion Eng. Des. 81 (2006) 2623–2631.

[15] H.-S. Chang, D.S. Park, J.J. Joo, K.M. Moon, K.W. Cho, Y.S. Kim, J.S. Bak, H.M. Kim, M.C. Cho, I.K. Kwon, E. Fauve, J.-M. Bernhardt, P. Dauguet, J. Beauvisage, F. Andrieu, S.-H. Yang, G.M. Gistau Baguer, The on-site status of the KSTAR helium refrigeration system, Adv. Cryog. Eng. Proc. Cryog. Eng. Conf. (2008) 1689–1699.

[16] https://www.iterkorea.org/eng/020605. (Accessed 17 June 2017).

[17] Private communication, 16 August 2017

[18] H. Bai, E.C. Group, Cryogenics in EAST Cryogenic distribution system, Fusion Eng. Des. 81 (2006) 1–7.

[19] S. Wu, An overview of the EAST project, Fusion Eng. Des. 82 (2007) 463–471.

[20] G.S. Xu, J.G. Li, B.N. Wan, P. Fu, H.Y. Guo, X.Z. Gong, EAST superconducting tokamak, AAPPS Bull. 23 (2013) 9–13.

[21] B. Sarkar, J. Tank, P. Panchal, A.K. Sahu, R. Bhattacharya, G. Phadke, N.C. Gupta, G. Gupta, N. Shah, P. Shukla, M. Singh, D. Sonara, R. Sharma, S. Saradha, J.C. Patel, Y.C. Saxena, Cryogenic system of steady state superconducting Tokamak SST-1: operational experience and controls, Fusion Eng. Des. 81 (2006) 2633–2641.

[22] Y. Saxena, Present status of the SST-1 project, Nucl. Fusion 40 (2000) 1069–1082.

[23] Stellarators difficult to build? The construction of Wendelstein 7-X. (Accessed 16 July 2018).

[24] Y. Bozhko, F. Schauer, Refrigeration system for W7-X, Nucl. Fusion 43 (2003) 835–841.

[25] M. Nagel, C.P. Dhard, H. Bau, H.-S. Bosch, U. Meyer, S. Raatz, K. Risse, T. Rummel, Cryogenic commissioning, cool down and first magnet operation of Wendelstein 7-X, IOP Conf. Ser. Mater. Sci. Eng. 171 (2017).

[26] R. Maekawa, K. Ooba, M. Nobutoki, T. Mito, Dynamic simulation of the helium refrigerator/liquefier for LHD, Cryogenics 45 (2005) 199–211.

[27] S. Satoh, T. Mito, S. Yamada, J. Yamamoto, O. Motojima, Construction of a 10 kW class helium cryogenic system for the large helical device, Cryogenics 34 (1994) 95–98.

[28] H. Katheder, Cryogenic needs for future tokamaks, ICEC- 14 (1992) 109–117.

[29] P. Komarek, Superconducting magnets in fusion research, Cryogenics 25 (1985) 604–612.

[30] Y. Iwasa, Case Studies in Superconducting Magnets, Springer US, Boston, MA, 2009.

[31] L. Bottura, Cable Stability, 2014, https://doi.org/10.5170/CERN-2014-005.401.

[32] V. Kalinin, E. Tada, F. Millet, N. Shatil, ITER cryogenic system, Fusion Eng. Des. 81 (2006) 2589–2595.

[33] L. Serio, H.-S. Chang, C. Parente, A. Forgeas, M. Chalifour, T. Voigt, E. Monneret, H. Vaghela, R. Bhattacharyay, S. Badgujar, N. Shah, B. Sarkar, N. Peng, Y. Xiong, L.,L. Liu, G. Gistau, The conceptual design of the ITER cryodistribution system, in: Proc. Twenty-Third Int. Cryog. Eng. Conf. Int. Cryog. Mater. Conf., 2011, 2010, pp. 1–30.

[34] H.-S. Chang, R. Maekawa, A. Forgeas, M. Clough, M. Chalifour, H. Vaghela, R. Bhattacharya, B. Sarkar, Optimization of the ITER cryodistribution for an efficient cooling of the magnet system, IEEE Trans. Appl. Supercond. 26 (2016).

[35] C. Day, D. Murdoch, R. Pearce, The vacuum systems of ITER, Vacuum 83 (2008) 773–778.

[36] K. Yoshida, K. Tsuchiya, K. Kizu, H. Murakami, K. Kamiya, M. Peyrot, P. Barabaschi, Design and construction of JT-60sa superconducting magnet system, J. Plasma Fusion Res. 9 (2010) 214–219. http://www.jspf.or.jp/JPFRS/PDF/Vol9/jpfrs2010_09-214.pdf.

[37] R. Heller, W.H. Fietz, M. Heiduk, M. Hollik, A. Kienzler, C. Lange, R. Lietzow, I. Meyer, T. Richter, T. Vogel, Overview of JT-60sa HTS current lead manufacture and testing, IEEE Trans. Appl. Supercond. 28 (2018) 1–5.

[38] G.H. Kim, W.C. Kim, H.L. Yang, E.N. Bang, K.P. Kim, K.S. Lee, H.T. Kim, Y.S. Kim, J.S. Bak, D.K. Kang, Y.S. Lee, KSTAR thermal shield, Fusion Eng. Des. 84 (2009) 1043–1048.

[39] V. Amoskov, A. Belov, V. Belyakov, O. Filatov, O. Ilyasov, V. Kalinin, M. Kaparkova, V. Kukhtin, N. Shatil, S. Sytchevsky, V. Vasiliev, Validation of VINCENTA modelling based on an experiment with the central solenoid model coil of the International Thermonuclear Experimental Reactor, Plasma Dev. Oper. 14 (2006) 47–59.

[40] D. Bessette, N. Shatil, E. Zapretilina, Simulations of the ITER toroidal field coil operation with the VINCENTA code, IEEE Trans. Appl. Supercond. 16 (2006) 795–798.

[41] F. Gauthier, D. Bessette, D.K. Oh, Thermal hydraulic analysis of the ITER PF and correction coils in 15 MA scenario operation using the SuperMagnet suite of codes, IEEE Trans. Appl. Supercond. 24 (2014).

[42] L. Savoldi Richard, F. Casella, B. Fiori, R. Zanino, The 4C code for the cryogenic circuit conductor and coil modeling in ITER, Cryogenics 50 (2010) 167–176.

[43] R. Bonifetto, A. Kholia, B. Renard, K. Riße, L.S. Richard, R. Zanino, Modeling of W7-X superconducting coil cool-down using the 4C code, Fusion Eng. Des. 86 (2011) 1549–1552.

[44] R. Bonifetto, P. Bruzzone, V. Corato, L. Muzzi, S. Member, L. Savoldi, B. Stepanov, R. Zanino, S. Member, A. Zappatore, Thermal-hydraulic test and analysis of the ENEA TF conductor sample for the EU DEMO fusion reactor, IEEE Trans. Appl. Supercond. 28 (2018).

[45] R. Zanino, D. Bessette, L.S. Richard, Quench analysis of an ITER TF coil, Fusion Eng. Des. 85 (2010) 752–760.

[46] R. Bonifetto, F. Casella, L. Savoldi Richard, R. Zanino, Dynamic modeling of a supercritical helium closed loop with the 4C Code, AIP Conf. Proc. 1434 (2012) 1743–1750.

[47] L. Savoldi Richard, R. Bonifetto, R. Heller, R. Zanino, Thermal-hydraulic simulation of 80 kA safety discharge in the ITER toroidal field model coil (TFMC) using the 4C code, IEEE Trans. Plasma Sci. 40 (2012) 782–787.

[48] L. Savoldi Richard, R. Bonifetto, S. Carli, M. Grand Blanc, R. Zanino, Modeling of pulsed heat load in a cryogenic SHe loop using Artificial Neural Networks, Cryogenics 57 (2013) 173–180.

[49] R. Zanino, R. Bonifetto, R. Heller, L. Savoldi Richard, Validation of the 4C thermal-hydraulic code against 25 kA safety discharge in the ITER Toroidal Field Model Coil (TFMC), IEEE Trans. Appl. Supercond. 21 (2011) 1948–1952.

[50] R. Zanino, R. Bonifetto, A. Brighenti, T. Isono, H. Ozeki, L. Savoldi, Prediction, experimental results and analysis of the ITER TF insert coil quench propagation tests, using the 4C code, Supercond. Sci. Technol. 31 (2018) 35004.

[51] W.M. Kays, No title, Trans. ASME. 77 (1955) 1295.
[52] F.P. Incropera, T.L. Bergman, A.S. Lavine, D.P. DeWitt, Fundamentals of Heat and Mass Transfer, John Wiley, 2011.
[53] R.F. Barron, Cryogenic Heat Transfer, Taylor & Francis, 1999.
[54] J.P. Holman, S. Bhattacharyya, Heat Transfer, tenth ed., McGraw Hill, 2002.
[55] S. Kakac, R.K. Shah, W. Aung, Handbook of Single-phase Convective Heat Transfer, John Wiley, New York, 1987.
[56] R.H. Winterton, No title, Int. J. Heat Mass Tran. 41 (1998) 809.
[57] E.N. Sieder, G.E. Tate, Heat transfer and pressure drop of liquids in tubes, Ind. Eng. Chem. 28 (1936) 1429–1435.
[58] V. Gnielinski, New equations for heat and mass transfer in turbulent pipe and channel flow, Int. Chem. Eng. 16 (1976) 359–368.
[59] B.S. Petukhov, Heat transfer and friction in turbulent pipe flow with variable physical properties, Adv. Heat Tran. (1970) 504–564.
[60] H. Hausen, Darstellung des Warmeuberganges in Rohren durch verallgeminerte Potenzbeziehungen, Z. Ver Deutsch. Ing Beih. Verfahrenstech. (1943) 91–98.
[61] R.D. McCarty, Thermodynamic properties of helium 4 from 2 to 1500 K at pressure to 108 Pa, J. Phys. Chem. Ref. Data 2 (1973) 119.
[62] R.F. Barron, Cryogenic Systems, 1985th ed., OUP USA; 2 Edition (22 August 1985), 1985.
[63] R.V. Smith, Review of heat transfer to helium I, Cryogenics 9 (1969) 11–19.
[64] P.J. Giarratano, V.D. Arp, R.V. Smith, Forced convection heat transfer to supercritical helium, Cryogenics 11 (1971) 385–393.
[65] V.G. Pron'ko, G.P. Malyshev, Modes of "normal" and "deteriorated" heat exchange in the single-phase near-critical region in the turbulent flow of helium in tube, Transl. from Inzhenerno-Fizicheskii Zhurnal 30 (1976) 606–612.
[66] H. Ogata, S. Sato, Forced convection heat transfer to boiling helium in a tube, Cryogenics 14 (1974) 375–380.
[67] D.J. Brassington, D.N.H. Cairns, Measurements of forced convective heat transfer to supercritical helium, Int. J. Heat Mass Tran. 20 (1977) 207–214.
[68] D.N.H. Cairns, D.J. Brassington, A pumped supercritical helium flow loop for heat transfer studies, Cryogenics 16 (1976) 465–468.
[69] V.A. Bogachev, V.M. Yeroshenko, O.F. Snyitina, L.A. Yaskin, Measurements of heat transfer to supercritical helium in vertical tubes under forced and mixed convection conditions, Cryogenics 25 (1985) 198–201.
[70] P.J. Giarratano, M.C. Jones, Deterioration of heat transfer to supercritical helium at 2·5 atmospheres, Int. J. Heat Mass Tran. 18 (1975) 649–653.
[71] D. Kasao, T. Ito, Review of existing experimental findings on forced convection heat transfer to supercritical, Cryogenics 29 (1989) 630–636.
[72] M. Hoenig, D. Montgomery, Dense supercritical-helium cooled superconductors for large high field stabilized magnets, IEEE Trans. Magn. 11 (1975) 569–572.
[73] S. Pradhan, Y.C. Saxena, B. Sarkar, G. Bansal, A.N. Sharma, K.J. Thomas, V. Bedakihale, B. Doshi, C.P. Dhard, U. Prasad, P. Rathod, R. Bahl, A. Varadarajulu, A. Mankani, Superconducting Magnets of SST-1 Tokamak, International Atomic Energy Agency (IAEA), 2005. http://inis.iaea.org/search/search.aspx?orig_q=RN:36080624.
[74] X. Cheng, W. Lehmann, Pressure drop and transveral heat transfer in Wendelstein 7-X superconductors, Cryogenics 34 (1994) 607–610.
[75] C. Marinucci, P. Bruzzone, A. Della Corte, L.S. Richard, R. Zanino, Pressure drop of the ITER PFCI cable-in-conduit conductor, IEEE Trans. Appl. Supercond. 15 (2005) 1383–1386.
[76] K. Hamada, T. Kato, K. Kawano, Experimental results of pressure drop measurement in ITER CS model coil tests, Adv. Cryog. Eng. Proc. Cryog. Eng. Conf. 47 (2002) 407–414.
[77] S. Nicollet, J.L. Duchateau, H. Fillunger, A. Martinez, Calculations of pressure drop and mass flow distribution in the toroidal field model coil of the ITER project, Cryogenics 40 (2000) 569–575.
[78] H. Katheder, Optimum thermohydraulic operation regime for cable in conduit superconductors (CICS), Cryogenics 34 (1994) 595–598.
[79] X. Cheng, Transversal heat transfer in the cable-in-conduit conductor for the Wendelstein 7-X magnet system, Cryogenics 34 (1994) 659–666.
[80] S. Nicollet, H. Cloez, J.L. Duchateau, J.P. Serries, Hydraulics of the ITER toroidal field model coil cable-in-conduit conductors. Symp. Fusion Technol., Association Euratom-CEA Cadarache, France, 1998. http://inis.iaea.org/search/search.aspx?orig_q=RN:31008042.
[81] S. Nicollet, J.L. Duchateau, H. Fillunger, A. Martinez, S. Parodi, Dual channel cable in conduit thermohydraulics: influence of some design parameters, IEEE Trans. Appl. Supercond. 10 (2000) 1102–1105.
[82] R. Zanino, P. Santagati, L. Savoldi, A. Martinez, S. Nicollet, Friction factor correlation with application to the central cooling channel of cable-in-conduit super-conductors for fusion magnets, IEEE Trans. Appl. Supercond. 10 (2000) 1066–1069.
[83] R. Zanino, L. Savoldi Richard, A review of thermal-hydraulic issues in ITER cable-in-conduit conductors, Cryogenics 46 (2006) 541–555.
[84] C. Marinucci, L. Bottura, P. Bruzzone, B. Stepanov, Analysis of the transverse heat transfer coefficients in a dual channel ITER-type cable-in-conduit conductor, Cryogenics 47 (2007) 563–576.
[85] M. Bagnasco, L. Bottura, M. Lewandowska, Friction factor correlation for CICC's based on a porous media analogy, Cryogenics 50 (2010) 711–719.
[86] M. Lewandowska, M. Bagnasco, Modified friction factor correlation for CICC's based on a porous media analogy, Cryogenics 51 (2011) 541–545.
[87] S. Nicollet, D. Ciazynski, J.L. Duchateau, B. Lacroix, B. Renard, Evaluation of the ITER cable in conduit conductor heat transfer, in: ICEC, 2004, pp. 589–592.
[88] L. Bottura, P. Bruzzone, C. Marinucci, B. Stepanov, Analysis of transverse heat transfer coefficient in CICC's with central cooling channel, Cryogenics 46 (2006) 597–605.
[89] R. Zanino, S. Giors, R. Mondino, CFD modeling of ITER cable-in-conduit superconductors. Part I: friction IN the central channel, Adv. Cryog. Eng. Proc. Cryog. Eng. Conf. (2006) 1009–1016.
[90] R. Zanino, S. Giors, R. Mondino, CFD modeling of ITER cable-in-conduit superconductors. Part II. Effects of spiral geometry on the central channel pressure drop, Fusion Eng. Des. 81 (2006) 2605–2610.
[91] R. Zanino, S. Giors, L. Savoldi Richard, Cfd modeling OF ITER cable-in-conduit super-conductors. Part III: correlation for the central channel friction factor, ICEC-21 (2006).
[92] D. Raja Sekhar, V.V. Rao, Three dimensional CFD analysis of Cable-in-Conduit Conductors (CICCs) using porous medium approach, Cryogenics 54 (2013) 20–29.
[93] R.S. Dondapati, V.V. Rao, Influence of mass flow rate on Turbulent Kinetic Energy (TKE) distribution in Cable-in-Conduit Conductors (CICCs) used for fusion grade magnets, Fusion Eng. Des. 88 (2013) 341–349.
[94] R.S. Dondapati, V.V. Rao, CFD analysis of cable-in-conduit conductors (CICC) for fusion grade magnets, IEEE Trans. Appl. Supercond. 22 (2012).
[95] D.R. Sekhar, V.V. Rao, B. Sarkar, R. Bahl, Hydraulic modelling of cable – in-conduit conductors (CICC): CFD approach, Indian J. Cryogenics 38 (2013) 2–7.
[96] M. Bagnasco, L. Bottura, P. Bruzzone, M. Lewandowska, C. Marinucci, F. Staehli, Pressure drop of cable-in-conduit conductors with different VOID fraction, AIP Conf. Proc. 53 (2008) 1317–1324.
[97] P. Bruzzone, Pressure drop and helium inlet in ITER CS1 conductor, Fusion Eng. Des. 58–59 (2001) 211–215.
[98] M. Lewandowska, L. Malinowski, Transverse heat transfer coefficient in the dual channel ITER TF CICCs. Part III: direct method of assessment, Cryogenics 73 (2016) 91–100.
[99] V. Hauer, J.C. Boissin, C. Day, H. Haas, A. Mack, D. Murdoch, R. Lässer, M. Wykes, Design of the ITER torus prototype cryopump, Fusion Eng. Des. 82 (2007) 2113–2119.
[100] C. Day, H. Haas, S. Hanke, V. Hauer, X. Luo, M. Scannapiego, R. Simon, H. Strobel, F. Fellin, R. Lässer, A. Masiello, S. Papastergiou, M. Dremel, C. Mayaux, R. Pearce, Design progress for the ITER torus and neutral beam cryopumps, Fusion Eng. Des. 86 (2011) 2188–2191.
[101] R. Gangradey, S.S. Mukherjee, P. Panchal, P. Nayak, J. Agarwal, C. Rana, S. Kasthurirengan, J.S. Mishra, H. Patel, P. Bairagi, V. Lambade, R. Sayani, Pumping speed offered by activated carbon at liquid helium temperatures by sorbents adhered to indigenously developed hydroformed cryopanel, IOP Conf. Ser. Mater. Sci. Eng. 101 (2015).
[102] K. S, V. G A, V. Ravi, U. Behera, S. Udgata, R. Gangradey, Performance studies of Cryocooler based cryosorption pumps with indigenous activated carbons for fusion applications, IOP Conf. Ser. Mater. Sci. Eng. (2017) 3.
[103] M. Scannapiego, C. Day, Experimental and CFD analyses of a thermal radiation shield dimple plate for cryogenic pump application Experimental and CFD analyses of a thermal radiation shield dimple plate for cryogenic pump application, IOP Conf. Ser. Mater. Sci. Eng. 101 (2015).
[104] S. Suhagiya, R.M. Srivastava, Performance evolution of conceptual designed of single panel cryopump, Int. J. Eng. Sci. Res. Technol. 1 (2012) 242–250.
[105] J.J. Chopra, S. Mukherjee, R. Gangradey, A. Mavani, J. Agarwal, Thermohydraulic analysis of hydroformed radiation shield plate, Indian J. Cryogenics 42 (2017).
[106] C.R. Sanghani, N. Raviprakash, R. Gangradey, Experimental validation with CFD analysis of radiation shield plate for cryopump application, J. Exp. Appl. Mech. 6 (2015) 1–4.